Modeling of the electrical conductivity, thermal conductivity, and specific heat capacity of VO_2

Jose Ordonez-Miranda,* Younès Ezzahri, Karl Joulain, and Jérémie Drevillon
Institut Pprime, CNRS, Université de Poitiers, ISAE-ENSMA, F-86962 Futuroscope Chasseneuil, France

J. J. Alvarado-Gil
Institut Pprime, CNRS, Université de Poitiers, ISAE-ENSMA, F-86962 Futuroscope Chasseneuil, France
and Departamento de Física Aplicada, Cinvestav-Unidad Mérida, Carretera Antigua a Progreso km. 6, 97310, Mérida, Yucatán, México

(Received 22 June 2018; revised manuscript received 28 July 2018; published 24 August 2018)

Based on Bruggeman's symmetric effective-medium formula and an explicit expression derived for the temperature evolution of the volume fractions of the metallic and isolating domains appearing during the heating and cooling of VO_2, respectively, we develop a model to describe the hysteresis of its electrical and thermal conductivities as well as of its specific heat capacity. The model takes into account the average value and standard deviation of the transition temperatures of the individual domains, as well as their activation energies, which represent the driving force for the existence of the VO_2 hysteresis. It is shown that the model's predictions driven by these three parameters related to the microstructure of VO_2 are in good agreement with robust experimental data. Furthermore, as these parameters are intrinsically correlated to the doping, defect, strain, and interface effects of VO_2, the proposed model enables the seamless integration of these effects, and therefore, its predictions are also expected to be useful for describing the thermal and electrical properties of composites based on VO_2.

DOI: 10.1103/PhysRevB.98.075144

I. INTRODUCTION

Vanadium dioxide (VO_2) is one of the most striking binary oxides and has attracted great interest for several decades [1–3] due to its hysteretic metal-insulator transition (MIT) around a critical temperature (∼342 K) near room temperature. This thermally induced MIT is driven by the transformation of the VO_2 crystal structure from a monoclinic unit cell in the low-temperature ($T < 340$ K) insulating phase to a tetragonal rutile one in the high-temperature ($T > 345$ K) metallic phase. As a result of this remarkable change of its structure and energy carriers, the electrical, optical, thermal, and magnetic properties of VO_2 exhibit sizable changes [1,4–7], which can be used for a wide variety of applications [2,8–10] involving the manipulation of electrical and heat currents to process information and efficiently manage the energy resources of nature. In particular, this is the case for the thermal diode, whose ability to rectify radiative current was recently demonstrated theoretically [11] and experimentally [12–14].

Experiments show that the physical properties of VO_2 are characterized by hysteresis, such that their values are different during the heating and cooling processes at a given temperature within the MIT [15–17]. Yang *et al.* [7] showed that the width of the hysteresis loop of the VO_2 electrical resistivity, sharpness of the transition, and transition temperature depend strongly on the epitaxial growth of VO_2 films on sapphire. This indicates that the substrate represents an effective way to tailor the overall properties of VO_2 films. On the other hand, thermal conductivity variations of VO_2 films were also measured by ultrafast pump-probe techniques [18,19]. The comprehension and physical description of the VO_2 MIT are very challenging because of the disordered coexistence of metallic and insulating phases involving multiple interactions among the electronic (charge, orbital, and spin) and lattice (phonon) degrees of freedom [20–22]. This is the reason why physical models to describe the hysteretic MIT of VO_2 are scarce and essentially empirical [5,23–26]. Based on the Preisach's theory [27], de Almeida *et al.* [23] proposed a model for the hysteresis of the VO_2 electrical resistance R in terms of six fitting parameters. More recently, Ramirez *et al.* [5] used the mean-field theory to derive another model for R by considering that the driving force in charge of opening the VO_2 hysteresis is the interaction between nearest-neighbor domains of the metallic and insulating phases. The predictions of these two multiparameter models [5,23] agree with some experimental data, but their application is restricted to the electrical resistance of VO_2. Other VO_2 physical properties are still missing a suitable theoretical description based on physically sound parameters related to the VO_2 microstructure [28], which is paramount to properly interpret VO_2 experimental data, tailor the physical properties of VO_2, and assess its practical applications.

In this work, we model the electrical and thermal conductivities of VO_2 as well as its specific heat capacity during its MIT. This is done by combining Bruggeman's symmetric effective-medium model with an explicit expression for the temperature evolution of the volume fraction of the metallic (insulating) domains that appears during the heating (cooling) of VO_2. The predictions of the proposed model depend on three parameters driven by the VO_2 microstructure and are in good agreement with various experimental data reported in the literature.

*jose.ordonez@cnrs.pprime.fr

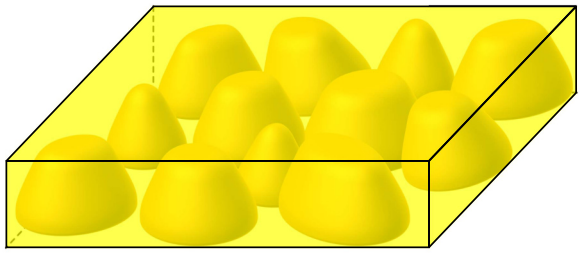

FIG. 1. Scheme of the metallic (insulating) domains that show up during the heating (cooling) of VO_2.

II. THEORETICAL MODELING

According to near-field images [15–17], as the temperature of VO_2 increases, its insulator-to-metal (heating) phase transition is driven by the nucleation, proliferation, and percolation of metallic domains inside the insulating host. On the other hand, during the metal-to-insulator (cooling) phase transition, the insulating domains nucleate in the metallic matrix, then proliferate, and finally percolate as the temperature decreases. As a result of the coexistence of both the metallic and insulating phases within the MIT, VO_2 can be considered a composite material made up of domains (particles) embedded in a matrix, as depicted in Fig. 1. The effective property χ (electrical conductivity or thermal conductivity) of VO_2 during its heating and cooling can then be modeled by Bruggeman's symmetric model, which considers the domains and matrix to be two symmetrical components of the composite, and therefore, it can be used for all volume fractions of domains. Another relevant feature of this model is its prediction of the percolation of χ for a certain volume fraction of particles [29,30], which is the case of the VO_2 properties at its transition temperature. Based on this fact, Bruggeman's symmetric model was previously used to model the VO_2 permittivity [31–33], and here we apply it for describing both the electrical conductivity ($\chi = \sigma$) and thermal conductivity ($\chi = k$) as follows:

$$f_m \frac{\chi_m - \chi}{\chi_m + (q^{-1} - 1)\chi} + f_i \frac{\chi_i - \chi}{\chi_i + (q^{-1} - 1)\chi} = 0, \quad (1)$$

where χ_m and χ_i are the corresponding VO_2 properties in its pure metallic and insulating phases, respectively, f_m and $f_i = 1 - f_m$ are the volume fractions of the metallic and insulating domains during the MIT, and q is the domains' depolarization factor along the direction in which the property χ is considered. This factor q is determined by the domains' shape, which drives the values of χ, as established by Eq. (1). For instance, for flat domains ($q = 1$), Eq. (1) yields the following cross plane χ of a VO_2 film: $1/\chi = f_m/\chi_m + f_i/\chi_i$, which is the well-known formula for domains with a spatial distribution in series. By contrast, for long cylindrical domains ($q = 0$), Eq. (1) reduces to the formula $\chi = f_m\chi_m + f_i\chi_i$ for domains in parallel. In practice, however, according to the near-field images taken by Qazilbash *et al.* [15,16] in VO_2 thin films, the factor q takes values mainly within the interval 0.2−0.4, which indicates that the domains evolve with temperature, keeping a nearly spherical shape ($q = 1/3$). This is reasonable for thin films much thicker than the domains' size, which is typically a few nanometers. In this condition, the birth and growth of the domains are not strongly affected by the film thickness, we can model χ with the average value $q = 1/3$, and the physical solution ($\chi > 0$) of Eq. (1) can be written as follows:

$$\chi = \frac{\alpha + \sqrt{\alpha^2 + 8\chi_m\chi_i}}{4}, \quad (2)$$

where $\alpha = (3f_m - 1)\chi_m + (3f_i - 1)\chi_i$. Equation (2) determines thus the effective property χ within the MIT, provided that its values in the insulating (χ_i) and metallic (χ_m) phases are known along with the temperature evolution of their volume fractions. Considering that the nth metallic domain appearing during the heating process of VO_2 at temperature T has a critical (minimum) temperature $T_c^{(n)}$ of appearance, the volume fraction $f_m(T)$ of all metallic domains can then be calculated by

$$f_m(T) = \int_0^\infty p_{\rm up}\big(T, T_c^{(n)}\big) D\big(T, T_c^{(n)}\big) dT_c^{(n)}, \quad (3)$$

where $p_{\rm up}(T, T_c^{(n)})$ is the existence probability of the metallic domains and $D(T, T_c^{(n)})$ is the distribution of their critical temperatures $T_c^{(n)}$, which we assume to be a Gaussian one ($D(T, T_c^{(n)}) = \exp[-(T_c^{(n)} - T_c)^2/(2\Delta T^2)]/(\sqrt{2\pi}\Delta T)$) centered at the VO_2 transition temperature T_c with a width (standard deviation) ΔT, as was considered previously [5]. This distribution describes well the size dispersion of the VO_2 domains along with their dynamical nature within the MIT [28,34], and its predictions agree well with experimental data, as shown below. Given that the metallic domains exist only for $T \geqslant T_c^{(n)}$, their probability of existence is determined by the Boltzmann distribution as follows: $p_{up} = H(T - T_c^{(n)}) \exp(-\Delta E^{(n)}/k_B T)$, where $H(\cdot)$ is the Heaviside step function, k_B is the Boltzmann constant, and $\Delta E^{(n)}$ is the energy barrier that the metallic domains need to overcome to appear inside the insulating matrix. If $k_B U$ is the energy required to make the first metallic domains appear, the average value of this energy barrier is then $\langle \Delta E^{(n)} \rangle = (1 - f_m)k_B U$, which explicitly shows that the energy required by the insulating phase to transform into the metallic one decreases as the metallic volume fraction increases. The combination of this energy activation with Eq. (3) yields

$$f_m(T) \exp\{[1 - f_m(T)]U/T\} = \frac{1}{2}\mathrm{erfc}\left(\frac{T_c - T}{\sqrt{2}\Delta T}\right), \quad (4)$$

where $\mathrm{erfc}(\cdot)$ is the complementary error function. In the limit of low (high) temperature $T \ll T_c$ ($T \gg T_c$), Eq. (4) reduces to $f_m = 0$ ($f_m = 1$), regardless of the energy barrier U (in K), as expected. On the other hand, if the energy barrier is very high ($U \gg T$), for all temperatures of interest, the metallic domains do not appear, and Eq. (4) predicts that $f_m = 0$. By contrast, for a low energy barrier ($U \ll T$), Eq. (4) becomes $f_m(T) = \mathrm{erfc}[(T_c - T)/(\sqrt{2}\Delta T)]/2 \approx 1 - 1/\{1 + \exp[5(T - T_c)/(2\sqrt{2}\Delta T)]\}$, which was empirically proposed and used in previous works [23,24,35–39]. Furthermore, note that for $T = T_c$, Eq. (4) reduces to $U/T_c = -\ln[2f_m(T_c)]/[1 - f_m(T_c)]$, which shows the direct relation between U and T_c and enables us to determine U, provided that $f_m(T_c)$ and T_c are known. Note that $f_m(T_c) = 1/2$ occurs only when the energy barrier is much smaller than the critical temperature ($U \ll T_c$). This transition temperature T_c for the property χ can be defined by $\partial\chi/\partial T\,|_{T=T_c} = 0$. Taking into

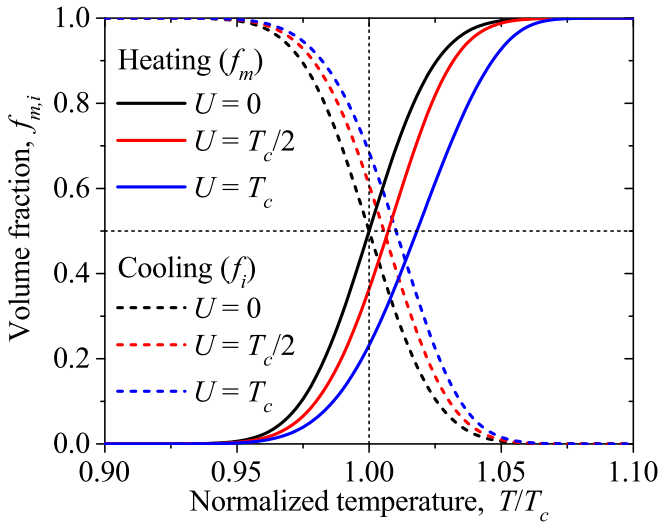

FIG. 2. Temperature evolution of the volume fractions of the metallic and isolating domains during the heating and cooling processes of VO_2, respectively. Calculations have been done for three energy barriers U and a typical $\Delta T = 0.02U$.

account that the right-hand side of Eq. (4) is positive and smaller than unity, the analytical solution of Eq. (4) can be expressed in terms of the main branch W_0 of the Lambert W function as follows:

$$f_m(T) = -\frac{T}{U} W_0\left[-\frac{U}{2T}\exp\left(-\frac{U}{T}\right)\mathrm{erfc}\left(\frac{T_c - T}{\sqrt{2}\Delta T}\right)\right]. \quad (5)$$

Given that W_0 is a built-in function of many calculation softwares (Wolfram *Mathematica*, MATLAB, PYTHON, etc.), Eq. (5) directly provides the temperature evolution of the volume fraction of the metallic domains, which is required to determine the effective property $\chi(T)$ through Eq. (2). The parameters $(U, T_c, \Delta T)$ can be calculated by fitting either Eq. (2) or Eq. (5) to proper experimental data measured during the heating process of VO_2. For the cooling process, on the other hand, the volume fraction $f_i(T)$ of the insulating domains appearing within the metallic matrix can be determined following the same procedure as the one used to derive Eq. (5). The final result is

$$f_i(T) = \frac{T}{U} W_0\left[\frac{U}{2T}\exp\left(-\frac{U}{T}\right)\mathrm{erfc}\left(\frac{T - T_c}{\sqrt{2}\Delta T}\right)\right], \quad (6)$$

where U is now the energy barrier that the isolating domains have to overcome to show up within the metallic matrix, and therefore, its value is expected to be different than that in Eq. (5). U thus represents the driving force responsible for the hysteresis of VO_2, which, along with the other fitting parameters T_c and ΔT, determines $f_i(T)$ for the cooling process of VO_2. Figure 2 shows the predictions of Eqs. (5) and (6) for the temperature evolution of the volume fractions of the metallic and isolating domains during the heating and cooling of VO_2, respectively. Note that both volume fractions take the value $1/2$ at a temperature T that increases with the energy barrier U through values slightly greater than T_c ($T \geqslant T_c$). The volume fractions take the value $f_m(T_c) = f_i(T_c) = 1/2$ only in the absence of energy barrier ($U = 0$), which is not consistent with experimental data, as was previously shown [5]. Equations (5) and (6) are thus expected to provide a physical description of the VO_2 hysteresis in terms of the three parameters $(U, T_c, \Delta T)$, whose corresponding values for the heating and cooling processes are different. The combination of Eq. (2) with Eqs. (5) and (6) hence allows us to determine the temperature evolution of the measurable property $\chi(T)$ for the insulator-to-metal and metal-to-insulator phase transitions. Even though the proposed model provides the volume fractions of both the metallic and insulating phases, it cannot be used to determine the contributions of each of these phases to $\chi(T)$ because Bruggeman's model in Eq. (1) is an effective-medium approximation that considers VO_2 a homogeneous medium with an effective property $\chi(T)$. The separation of these contributions could be possible by other theories taking into account the inhomogeneous nature of VO_2 at the domains' level.

The volume fractions f_n of the metallic ($n = m$) and insulating ($n = i$) domains in Eqs. (5) and (6) can also be used to describe the temperature evolution of the specific heat capacity $c_{p,l}(T)$ of VO_2 at constant pressure during its heating ($l = \mathrm{up}$) and cooling ($l = \mathrm{down}$) processes, respectively. Taking into account that inside the MIT $c_{p,l}(T)$ changes sharply [1,36], while outside the MIT its values are determined mainly by the lattice contribution [4], the specific heat capacity of VO_2 at temperature T can be written as follows:

$$c_{p,l}(T) = c_D(T) + T\frac{\alpha_l^2}{\rho\beta_l} + L_l\frac{df_n}{dT}, \quad (7)$$

where $n = m$ ($n = i$) for $l = \mathrm{up}$ ($l = \mathrm{down}$), $c_D(T)$ is the specific heat capacity predicted by the Debye model, ρ is the density of VO_2, and L_l, α_l, and β_l are its latent heat, coefficient of thermal expansion, and isothermal compressibility for its dielectric-to-metal ($l = \mathrm{up}$) and metal-to-insulator ($l = \mathrm{down}$) transitions, respectively. For the heating process of VO_2 samples with high purity, the latent heat is $L_{\mathrm{up}} \approx 1020$ cal mol^{-1} [4], which is expected to result from the combined contributions of the phonons and electrons coexisting within the MIT. The second term on the right-hand side of Eq. (7) has been added to properly compare the specific heat capacity at constant volume $c_D(T)$ with the specific heat capacity at constant pressure $c_{p,l}(T)$, which is usually measured for solid-state materials. Taking into account that the experimental values of this second term are comparable to or smaller than 0.55 cal mol^{-1} K^{-1} [40], which is much smaller than the values ($\sim$14 cal mol^{-1} K^{-1}) of $c_D(T)$ for temperatures within the MIT [4], its contribution is going to be neglected in this work.

III. RESULTS AND DISCUSSION

We now apply the proposed model in Eq. (2) to describe the temperature dependence of the electrical conductivity σ, electrical resistance R, thermal conductivity k, and specific heat capacity c of VO_2. This is done by fitting our theoretical model to the experimental data reported in the literature for either σ, R, k, or c and treating the three parameters $(U, T_c, \Delta T)$ as fitting parameters. The values of these parameters thus determined are therefore supported by experimental data and are summarized in Table I.

The temperature evolution of the dc electrical conductivity σ of VO_2 is shown in Fig. 3 for the heating and cooling processes inside the MIT. The points represent the experimental

TABLE I. Fitting parameters involved in Eqs. (5) and (6).

	Cooling (Heating)		
	U (K)	T_c (K)	ΔT (K)
dc electrical conductivity	13.5 (323.7)	318.2 (326.2)	5.1 (5.5)
Electrical resistance	10.1 (233.2)	334.7 (342.5)	0.8 (1.0)
Thermal conductivity	10.1 (233.2)	334.5 (342.5)	0.8 (1.0)

data reported by Samanta *et al.* [34], while the solid lines stand for the theoretical predictions of Eq. (2) with $\sigma_m = 84175.1\,\mathrm{S\,m^{-1}}$, $\sigma_i = 4.86 \times 10^6 \exp(-3136.1/T)\,\mathrm{S\,m^{-1}}$ [34], and the fitting parameters summarized in Table I for the dc electrical resistance. Note that the energy $U = 323.7$ K (0.03 eV) required by the metallic domains to appear inside the insulating matrix is much greater than the one needed by the insulating domains to show up within the metallic matrix. This fact indicates that the binding energy of the atoms in the monoclinic insulating phase of VO_2 is higher than that of the atoms in its tetragonal metallic phase, as was reported in the literature [41,42]. Furthermore, this energy barrier for the heating process is consistent with literature values [5] and one order of magnitude smaller than the energy (0.6–0.7 eV) required to complete the whole insulator-to-metal transition [4]. On the other hand, Table I also shows that the transition temperature for the heating process is 8 K higher than that during the cooling one, which determines the hysteresis of σ in Fig. 3. More importantly, the theoretical predictions of Eq. (2) are in good agreement with the experimental data for both the heating and cooling processes, which indicates that our model can be applied to describe the full transition of the dc electrical conductivity of VO_2.

Figure 4 shows the comparison between the experimental [16] and theoretical values of the VO_2 electrical resistance

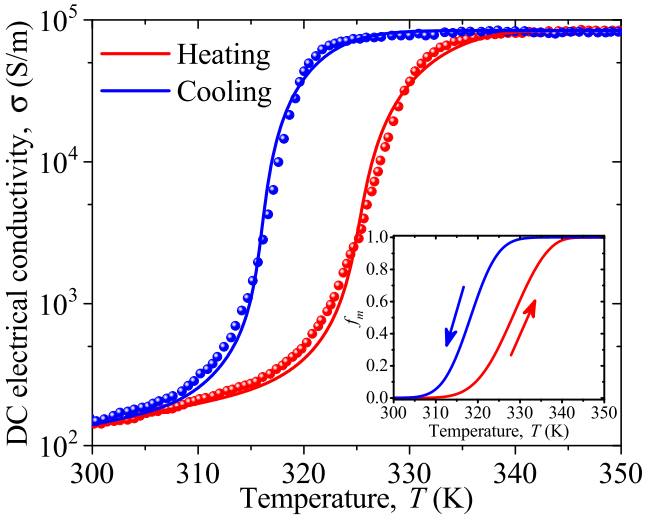

FIG. 3. Temperature evolution of the dc electrical conductivity σ of VO_2 within its MIT. The solid lines were obtained by fitting Eq. (2) ($\sigma = \chi$) to the experimental data reported by Samanta *et al.* [34]. The inset shows the hysteresis of the metallic volume fraction that drives the values of σ.

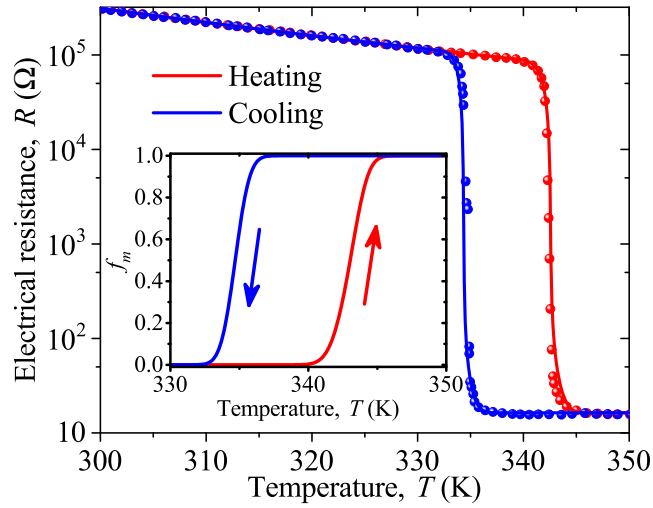

FIG. 4. Electrical resistance R of VO_2 as a function of its temperature. The solid lines were obtained by fitting Eq. (2) [$R = l/(A\chi)$] to the experimental data measured by Qazilbash *et al.* [16] for a VO_2 thin film of length l and cross section A. The inset shows the hysteresis of the metallic volume fraction that leads the behavior of R for the heating and cooling processes.

($R \propto \sigma^{-1}$) as a function of the temperature during the heating and cooling processes. The solid lines represent the predictions of Eq. (2) with $R_m = 16.33\ \Omega$, $R_i = 7.33 \exp(3197.61/T)\ \Omega$ [23,34], and the fitting parameters reported in Table I for the electrical resistance. Note that the values of these parameters are different from the corresponding ones found for the dc electrical conductivity shown in Fig. 3. This difference can be explained by the different techniques and substrates used by Samanta *et al.* [34] and Qazilbash *et al.* [16] for depositing the VO_2 samples and measuring the values of σ and R, respectively. Despite these dissimilarities, the difference between the critical temperatures for the heating and cooling processes (hysteresis width) is practically the same (8 K) for both σ and R, as shown in Table I and the insets of Figs. 3 and 4. The quite good agreement between the experimental and theoretical results shows the suitable predictive performance of our model to describe the temperature evolution of the VO_2 electrical resistance within the MIT. This fact also holds for the VO_2 thermal conductivity k, as shown in Figs. 5(a) and 5(b), for the heating process. The points stand for the experimental data reported by Oh *et al.* [18] and Qazilbash *et al.* [16,17] for k and f_m, respectively, while the lines represent their corresponding theoretical values predicted by Eqs. (2) and (5), with the three fitting parameters (U, T_c, ΔT) summarized in Table I. For the cooling process, the transition temperature T_c has been shifted 8 K downwards to take into account the experimentally observed thermal hysteresis of VO_2 [16]. Note that the temperature dependence of f_m thus obtained along with Eq. (2) describes quite well the experimental values of k, which shows the consistence between the data reported by Oh *et al.* [18] and Qazilbash *et al.* [16,17] and illustrates the good predictive performance of the proposed model to describe the thermal conductivity of VO_2. We did not consider the effect of the interface thermal resistance between the metallic and insulating domains because of the sharp phase transition (large

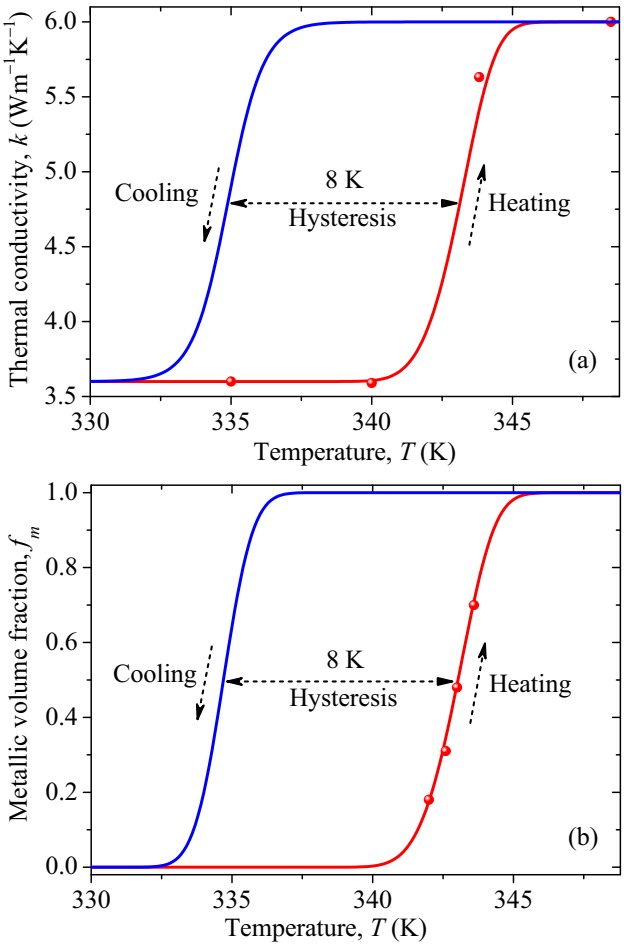

FIG. 5. Temperature evolution of (a) k and (b) f_m during the heating and cooling processes of VO_2. The points stand for the experimental data reported by Oh *et al.* [18] and Qazilbash *et al.* [16,17] for k and f_m, respectively, while the lines represent their corresponding theoretical values predicted by Eqs. (2) and (5), with $k_m = 6\ \mathrm{W\,m^{-1}\,K^{-1}}$, $k_i = 3.6\ \mathrm{W\,m^{-1}\,K^{-1}}$, and the fitting parameters summarized in Table I for k. The lines for the cooling process have been determined by shifting the transition temperature 8 K downwards from the heating one to take into account the experimentally observed thermal hysteresis [16].

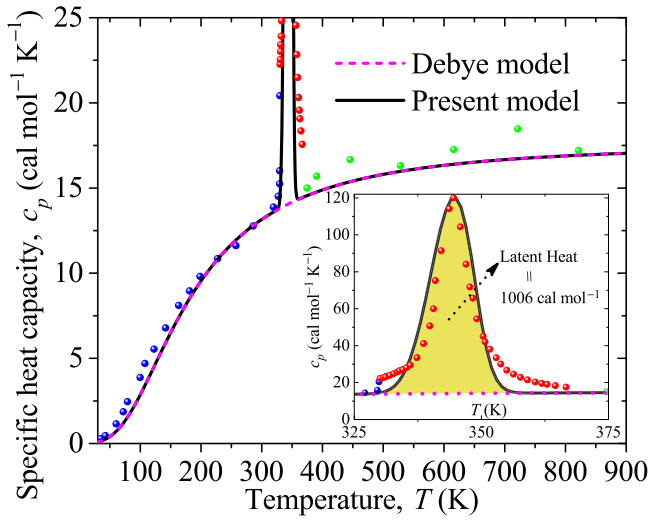

FIG. 6. Specific heat capacity c_p of VO_2 as a function of temperature during its heating process. The blue, red, and green points stand for the experimental data measured by Berglund and Guggenheim [4], Kawakubo and Nakagawa [1], and Cook [52], respectively, while the black solid line represents the prediction of Eq. (7).

$1/\Delta T$) of the VO_2 thermal conductivity, as shown in Fig. 5(a). This indicates that the average temperature difference ΔT of these domains is relatively small in comparison with their average temperature around T_c, as confirmed by the values of these parameters in Table I. This is the reason why the temperature jumps (thermal resistance effect) at the interfaces of the domains can be neglected, as done in Eq. (2) with $\chi = k$.

It is worth pointing out that to test our theoretical model, we have chosen the thermal conductivity data reported by Oh *et al.* [18] for polycrystalline VO_2 thin films because we know the average depolarization factor ($q \approx 1/3$) [16,17] of the VO_2 domains for this geometry and their data are consistent with the corresponding ones measured by Kizuka *et al.* [43]. According to Eq. (1), the predictions of the proposed model depend on this factor, whose values for other geometries are unknown to the best of our knowledge. Taking into account that the VO_2 geometry and crystallinity affect the appearance and growth of the metallic (insulating) domains inside the insulating (metallic) matrix during the heating (cooling) process of VO_2 across its MIT, VO_2 samples with different geometries are expected to exhibit distinct physical properties. For instance, based on the vapor-transport method, Lee *et al.* [2] grew single-crystalline VO_2 nanobeams with a nearly constant diameter and thermal conductivity practically independent of temperature across their phase transition. These experimental data for k contrast with the ones reported by Zhu *et al.* [44] for single-crystalline VO_2 nanobeam growth with the same technique but with a variable diameter tapered in shape. The latter authors found that the VO_2 thermal conductance (and hence the thermal conductivity) does vary with temperature; however, this variation is different from the one reported by Oh *et al.* [18] for polycrystalline VO_2 thin films. This fact confirms that the geometry and crystallinity of the VO_2 samples affect their thermal conductivity. The proposed model takes into account the geometry effect through the depolarization factor q and the crystallinity one through the VO_2 transition sharpness $1/\Delta T$, which increases with the degree of crystallinity [45].

The VO_2 specific heat capacity c_p at constant pressure is shown in Fig. 6 as a function of the temperature and for the heating process. By fitting the Debye model (violet dashed line) to the experimental data reported by Berglund and Guggenheim [4] for low temperatures ($T < 300$ K), we have found a Debye temperature $\Theta = 750$ K, which is about twice the critical temperature ($T_c = 342.5$ K) reported in the literature [4,42]. The scarce data (green points) for temperatures just above T_c prevent the determination of the Debye temperature in the metallic phase; however, the relatively small derivation of the violet dashed line from the green points indicates that its value should be similar to $\Theta = 750$ K. Within the MIT, the predictions of Eq. (7) with the metallic volume fraction $f_m(T)$ reported by Qazilbash *et al.* [16] (Fig. 5) are in fairly good agreement with the experimental data reported by Kawakubo and Nakagawa [1]. This striking consistence between the data

reported by two research groups 45 years apart for different properties of VO_2 provides an indication of the high quality of their VO_2 samples. Based on the predictions of the present and Debye models shown in Fig. 6, the latent heat (area inside the peak) of the transition is $L_{up} = 1006$ cal mol^{-1}, which is consistent with previous values reported in the literature [1,4]. Most importantly, the agreement between theory and experiment shows that Eq. (7) can be used to describe the specific heat capacity of VO_2 for temperatures inside and outside the MIT.

The fact that the temperature dependences of the volume fractions of the metallic $[f_m(T)]$ and insulating $[f_i(T)]$ domains of VO_2, combined with Bruggeman's model, can describe both smooth (Figs. 3, 4, and 5) and sharp (Fig. 6) temperature variations indicates the suitability of the proposed model to describe, in a unified way, both the electrical and thermal properties of VO_2. Therefore, given that both $f_m(T)$ and $f_i(T)$ have rigorously been derived based on concepts of statistical mechanics, as detailed in Sec. II, and are analytically expressed in Eqs. (5) and (6), respectively, they represent the main contribution to the proposed model. Furthermore, taking into account that the energy barrier U and/or the transition temperature T_c are directly correlated to the doping, defect, strain, and interface effects of VO_2 [45], the simple but efficient model in Eqs. (2) and (5)–(7) enables the seamless integration of these effects, and therefore, it could also be applied for describing the complex behavior of the electrical and thermal conductivities as well as the heat capacity of composites based on VO_2.

Taking into account that both the critical temperature T_c and transition sharpness $(1/\Delta T)$ can directly be deduced from the experimental data [46], while the energy barrier U can be determined only by fitting, the values of U can be estimated by applying the proposed model. These three parameters drive the VO_2 MIT and can be regulated by means of the following effects:

Doping effect. One efficient method to lower U and T_c is by doping VO_2 with W, as was experimentally found for $V_{1-x}W_xO_2$ films [47]. As the tungsten doping content x increases, these parameters linearly decrease as a result of the increasing disordered distribution of atoms and the detwisting of the V-V bonds [48].

Defects effect. The transition width $\Delta T \propto D_d$ is proportional to the defect density D_d (defect content per unit volume), including point defects, clusters, impurities, dislocations, and grain boundaries [45,49]. The impact of these latter planar defects is expected to strengthen for smaller nanograins, given that the surface area/volume ratio of grains increases as their sizes decrease. Therefore, sharper transitions (smaller ΔT) can be obtained with larger grains, as was experimentally observed by Narayan and Bhosle [45].

Strain/stress effect. The stresses and strains in VO_2 thin films, particularly epitaxial ones, shift the transition temperature T_c and transition width ΔT to lower values [4]. This effect can be generated by a suitable choice of the substrate and thin film processing parameters, as reported in the literature [50,51].

Based on these three effects, it is clear that the proposed model, whose predictions are driven by the three parameters $(U, T_c, \Delta T)$, can be used to predict not only the doping (energy barrier) required but also the microstructure needed to tailor the VO_2 properties for a particular application. Thus, this model establishes a fundamental correlation between the structure of VO_2 and its physical properties, which is essential to develop predictive capabilities.

IV. CONCLUSIONS

We have developed a model to describe the temperature evolution and hysteresis of the electrical and thermal conductivities as well as the specific heat capacity of VO_2 within its metal-insulator transition. This has been achieved by deriving an explicit expression for the volume fractions of the metallic and insulating domains in terms of their average transition temperature, the associated standard deviation, and their energy barriers inside the insulating and metallic matrices, respectively. By determining the values of these three physical parameters related to the microstructure of VO_2, we have shown that the physically sound predictions of the proposed model are in good agreement with convincing experimental data. This analytical model enables us to take into account the doping, defect, strain, and interface effects of VO_2, and therefore, its predictions are expected to be useful for describing the electrical and thermal properties of VO_2.

ACKNOWLEDGMENT

This work has been supported by the Cellule Énergie du CNRS through the Grant No. 267745.

[1] T. Kawakubo and T. Nakagawa, J. Phys. Soc. Jpn. **19**, 517 (1964).
[2] S. Lee, K. Hippalgaonkar, F. Yang, J. Hong, C. Ko, J. Suh, K. Liu, K. Wang, J. J. Urban, X. Zhang, C. Dames, S. A. Hartnoll, O. Delaire, and J. Wu, Science **355**, 371 (2017).
[3] J. Ordonez-Miranda, Y. Ezzahri, J. Drevillon, and K. Joulain, Phys. Rev. Appl. **6**, 054003 (2016).
[4] C. N. Berglund and H. J. Guggenheim, Phys. Rev. **185**, 1022 (1969).
[5] J.-G. Ramirez, A. Sharoni, Y. Dubi, M. E. Gomez, and I. K. Schuller, Phys. Rev. B **79**, 235110 (2009).
[6] J. Cao, W. Fan, H. Zheng, and J. Wu, Nano Lett. **9**, 4001 (2009).
[7] T.-H. Yang, R. Aggarwal, A. Gupta, H. Zhou, R. J. Narayan, and J. Narayan, J. Appl. Phys. **107**, 053514 (2010).
[8] J. Ordonez-Miranda, J. M. Hill, K. Joulain, Y. Ezzahri, and J. Drevillon, J. Appl. Phys. **123**, 085102 (2018).
[9] J. Ordonez-Miranda, Y. Ezzahri, J. Drevillon, and K. Joulain, J. Appl. Phys. **119**, 203105 (2016).
[10] H. Prod'homme, J. Ordonez-Miranda, Y. Ezzahri, J. Drevillon, and K. Joulain, J. Appl. Phys. **119**, 194502 (2016).
[11] P. Ben-Abdallah and S.-A. Biehs, Appl. Phys. Lett. **103**, 191907 (2013).
[12] A. Fiorino, D. Thompson, L. Zhu, R. Mittapally, S.-A. Biehs, O. Bezencenet, N. El-Bondry, S. Bansropun, P. Ben-Abdallah, E. Meyhofer, and P. Reddy, ACS Nano **12**, 5774 (2018).

[13] Z. Chen, C. Wong, S. Lubner, S. Yee, J. Miller, W. Jang, C. Hardin, A. Fong, J. E. Garay, and C. Dames, Nat. Commun. **5**, 5446 (2014).
[14] K. Ito, K. Nishikawa, H. Iizuka, and H. Toshiyoshi, Appl. Phys. Lett. **105**, 253503 (2014).
[15] M. M. Qazilbash, A. Tripathi, A. A. Schafgans, B.-J. Kim, H.-T. Kim, Z. Cai, M. V. Holt, J. M. Maser, F. Keilmann, O. G. Shpyrko, and D. N. Basov, Phys. Rev. B **83**, 165108 (2011).
[16] M. M. Qazilbash, M. Brehm, G. O. Andreev, A. Frenzel, P.-C. Ho, B.-G. Chae, B.-J. Kim, S. J. Yun, H.-T. Kim, A. V. Balatsky, O. G. Shpyrko, M. B. Maple, F. Keilmann, and D. N. Basov, Phys. Rev. B **79**, 075107 (2009).
[17] M. M. Qazilbash *et al.*, Science **318**, 1750 (2007).
[18] D.-W. Oh, C. Ko, S. Ramanathan, and D. G. Cahill, Appl. Phys. Lett. **96**, 151906 (2010).
[19] V. N. Andreev, F. A. Chudnovskii, A. V. Petrov, and E. I. Terukov, Phys. Status Solidi (a) **48**, K153 (1978).
[20] Y. Chang, C. Koo, J. Yang, Y. Kim, D. Kim, J. Lee, T. Noh, H.-T. Kim, and B. Chae, Thin Solid Films **486**, 46 (2005).
[21] T. J. Huffman, D. J. Lahneman, S. L. Wang, T. Slusar, B.-J. Kim, H.-T. Kim, and M. M. Qazilbash, Phys. Rev. B **97**, 085146 (2018).
[22] J. G. Ramirez, T. Saerbeck, S. Wang, J. Trastoy, M. Malnou, J. Lesueur, J. P. Crocombette, J. E. Villegas, and I. K. Schuller, Phys. Rev. B **91**, 205123 (2015).
[23] L. A. L. de Almeida, G. S. Deep, A. M. Nogueira-Lima, and H. Neff, Opt. Eng. **41**, 2582 (2002).
[24] L. A. L. de Almeida, G. S. Deep, A. M. N. Lima, I. A. Khrebtov, V. G. Malyarov, and H. Neff, Appl. Phys. Lett. **85**, 3605 (2004).
[25] D. J. Hilton, R. P. Prasankumar, S. Fourmaux, A. Cavalleri, D. Brassard, M. A. El Khakani, J. C. Kieffer, A. J. Taylor, and R. D. Averitt, Phys. Rev. Lett. **99**, 226401 (2007).
[26] G. Kotliarand and D. Vollhardt, Phys. Today **57**(3), 53 (2004).
[27] F. Preisach, Z. Phys. **94**, 277 (1935).
[28] V. A. Klimov *et al.*, Solid State Electron. **47**, 1134 (2002).
[29] J. Rozen, R. Lopez, R. F. Haglund, and L. C. Feldman, Appl. Phys. Lett. **88**, 081902 (2006).
[30] S. Kirkpatrick, Rev. Mod. Phys. **45**, 574 (1973).
[31] H. S. Choi, J. S. Ahn, J. H. Jung, T. W. Noh, and D. H. Kim, Phys. Rev. B **54**, 4621 (1996).
[32] J. B. Goodenough, J. Solid State Chem. **3**, 490 (1971).
[33] P. U. Jepsen, B. M. Fischer, A. Thoman, H. Helm, J. Y. Suh, R. Lopez, and R. F. Haglund, Phys. Rev. B **74**, 205103 (2006).
[34] S. Samanta, A. K. Raychaudhuri, X. Zhong, and A. Gupta, Phys. Rev. B **92**, 195125 (2015).
[35] K. Joulain, Y. Ezzahri, J. Drevillon, and P. Ben-Abdallah, Appl. Phys. Lett. **106**, 133505 (2015).
[36] X. Zhong, X. Zhang, A. Gupta, and P. LeClair, J. Appl. Phys. **110**, 084516 (2011).
[37] X. Zhong, P. LeClair, S. K. Sarker, and A. Gupta, Phys. Rev. B **86**, 094114 (2012).
[38] K. Ito, K. Nishikawa, and H. Iizuka, Appl. Phys. Lett. **108**, 053507 (2016).
[39] H. Prod'homme, J. Ordonez-Miranda, Y. Ezzahri, J. Drevillon, and K. Joulain, J. Quant. Spectrosc. Radiat. Transf. **210**, 52 (2018).
[40] G. Chandrashekhar, H. Barros, and J. Honig, Mater. Res. Bull. **8**, 369 (1973).
[41] T. Kawakubo, J. Phys. Soc. Jpn. **20**, 516 (1965).
[42] P. William, Mater. Res. Bull. **5**, 691 (1970).
[43] H. Kizuka, T. Yagi, J. Jia, Y. Yamashita, S. Nakamura, N. Taketoshi, and Y. Shigesato, Jpn. J. Appl. Phys. **54**, 053201 (2015).
[44] J. Zhu, K. Hippalgaonkar, S. Shen, K. Wang, Y. Abate, S. Lee, J. Wu, X. Yin, A. Majumdar, and X. Zhang, Nano Lett. **14**, 4867 (2014).
[45] J. Narayanand V. M. Bhosle, J. Appl. Phys. **100**, 103524 (2006).
[46] C. L. Gomez-Heredia, J. Ramirez-Rincon, J. Ordonez-Miranda, O. Ares, J. J. Alvarado-Gil, C. Champeaux, F. Dumas-Bouchiat, Y. Ezzahri, and K. Joulain, Sci. Rep. **8**, 8479 (2018).
[47] P. Jinand S. Tanemura, Jpn. J. Appl. Phys. **34**, 2459 (1995).
[48] X. Tan, T. Yao, R. Long, Z. Sun, Y. Feng, H. Cheng, X. Yuan, W. Zhang, Q. Liu, C. Wu, Y. Xie, and S. Wei, Sci. Rep. **2**, 466 (2012).
[49] K. Appavoo, D. Y. Lei, Y. Sonnefraud, B. Wang, S. T. Pantelides, S. A. Maier, and R. F. Haglund, Nano Lett. **12**, 780 (2012).
[50] L. Kang, Y. Gao, Z. Zhang, J. Du, C. Cao, Z. Chen, and H. Luo, J. Phys. Chem. C **114**, 1901 (2010).
[51] A. Tiwari, C. Jin, and J. Narayan, Appl. Phys. Lett. **80**, 4039 (2002).
[52] O. A. Cook, J. Am. Chem. Soc. **69**, 331 (1947).